Solid State Sciences 151 (2024) 107497

Contents lists available at ScienceDirect

Solid State Sciences

journal homepage: www.elsevier.com/locate/ssscie

Modification of tetrahedrite $Cu_{12}Sb_4S_{13}$ thermoelectric performance via the combined treatment of mechanochemistry and composite formation

Peter Baláž [a], Arda Baran Burcak [b], Umut Aydemir [b], Andrzej Mikula [c], Pawel Nieroda [c], Matej Baláž [a], Lenka Findoráková [a], Radovan Bureš [d], Viktor Puchý [d], Murat Erdemoglu [e], Marcela Achimovičová [a,*], Emmanuel Guilmeau [f], Sandy Al Bacha [f]

[a] Institute of Geotechnics, Slovak Academy of Sciences, Watsonova 45, 04353, Košice, Slovakia
[b] Koc University, Rumelifeneri Youlu, Sariyer, Istanbul, 34450, Turkey
[c] AGH University of Krakow, Faculty of Materials Science and Ceramics, al. Mickiewicza 30, 30-059, Krakow, Poland
[d] Institute of Materials Research, Slovak Academy of Sciences, Watsonova 47, 04001, Košice, Slovakia
[e] Inonu University, Engineering Faculty, Merkez Campus, 44280, Malatya, Turkey
[f] CRISMAT, CNRS, Normandie University, ENSICAEN, UNICAEN, 14000, Caen, France

ARTICLE INFO

Keywords:
Tetrahedrite
Chalcopyrite
Muscovite
Composite
Mechanochemistry
Thermoelectrics

ABSTRACT

Tetrahedrite $Cu_{12}Sb_4S_{13}$ with its low thermal conductivity represents a flagship in sulphide thermoelectrics. However, to achieve a reasonable figure-of-merit *ZT* (measure of thermoelectric efficiency), adequate doping or special sample processing is needed. In this work, a different approach (without doping) is illustrated for the two tetrahedrite-containing systems. *In the first approach* binary composite tetrahedrite $Cu_{12}Sb_4S_{13}$/chalcopyrite $CuFeS_2$ was prepared by *mechanochemical leaching* with the aim to obtain partly decomposed tetrahedrite. In this approach, the alkaline leaching medium (Na_2S + NaOH) was applied to extract Sb from tetrahedrite thus changing its composition. The obtained composite (formed from its own phases in an intrinsic mode) shows low values of $ZT = 0.0022@673$ K in comparison with the non-treated tetrahedrite where *ZT* was 0.0090@673 K. In this case the extremely high electric resistivity (6–20 mΩ cm^{-1}) was documented. *In the second approach* binary composite tetrahedrite $Cu_{12}Sb_4S_{13}$/muscovite $KAl_2(AlSi_3O_{10})(OH)_2$ (formed from its own and foreign phases in an extrinsic mode) was prepared by two-step *mechanical activation* in which combined treatment of industrial vibratory milling and subsequent laboratory planetary milling was applied. The addition of a foreign phase, muscovite, did not give extraordinary thermoelectric performance results. However, the two-step milling process (without the addition of foreign phase) gives the value of $ZT = 0.752@673$ K which belongs to the highest in the tetrahedrite thermoelectric community. In this case, the two-times increase in specific surface area and the increased amount of tetrahedrite in comparison to famatinite are suspectable for this effect. Both applied non-traditional approaches to synthesize tetrahedrite composites form a platform for potential modification of its thermoelectric performance.

1. Introduction

In nature, tetrahedrite belongs to one of the most widespread sulfosalts. Its general formula is $(Cu,Ag)_{10}(Cu,Zn,Fe,Cd,Hg)_2(Sb,As,Bi)_4S_{13}$. In metallurgy, tetrahedrites represent the most important source of Cu and Sb and are also of economic interest due to their content of Ag and Hg [1]. However, the processing of tetrahedrite ores is problematic because obtaining the main metal components (Cu and Sb) requires special operations such as intensification (the high-energy milling by mechanochemistry showed to be useful) and selective separation of Cu and Sb metals (alkaline leaching showed to be effective) [2].

In this situation, a new agenda for tetrahedrite utilization in the non-metallurgical field is strongly desirable. After the discovery of its low thermal conductivity [3], a challenge for its use in the energy sector as a new thermoelectric material seemed to be very promising. The synthetic mineral fulfils the criteria for high-performance thermoelectrics [4] with a large unit cell and Cu rattling in CuS_3 triangular planar coordinations [5]. To improve its transport properties, different

* Corresponding author.
E-mail address: achimovic@saske.sk (M. Achimovičová).

https://doi.org/10.1016/j.solidstatesciences.2024.107497
Received 21 December 2023; Received in revised form 21 February 2024; Accepted 3 March 2024
Available online 8 March 2024
1293-2558/© 2024 The Authors. Published by Elsevier Masson SAS. This is an open access article under the CC BY-NC-ND license (http://creativecommons.org/licenses/by-nc-nd/4.0/).

approaches are studied. In principle, bearing in mind that the dimensionless figure of merit $ZT = S^2\sigma T/\kappa$ [6], the focus is concentrated on maximizing of Seebeck coefficient (S) and electrical conductivity (σ) and minimizing thermal conductivity (κ). Carrier concentration tuning and phonon engineering have been reported as efficient strategies to improve TE properties of tetrahedrite [7,8].

Mechanochemistry via high-energy milling [2,9–13] with its capability to form lattice strain, defects and nanodimensional particles, creates a great potential in solid-state chemistry. Several modes can be applied. In *mechanical activation* (MA), only changes in physico-chemical properties (without changes in chemical composition) are manifested. On the contrary, in *mechanochemical leaching* (ML) and/or *mechanochemical synthesis* (MS), new compounds can be generated.

Mechanochemistry was shown to be effective also in the preparation of thermoelectric materials [14]. Its positive effect on tetrahedrite thermoelectricity by combining high-energy milling with spark plasma sintering was already documented (see Ref. [15] and papers cited within). The results for tetrahedrite were even obtained by high-energy milling in an industrial scale [16].

In the continuous tendency to improve the efficiency of thermoelectric materials, the development of composites seems to be a promising option. The formation of nanocomposites serves as a good example for making phase boundaries which creates the possibility of an additional phonon scattering mechanism and thus decreases the lattice thermal conductivity [17]. The defect-related interface and surface effects can contribute to *ZT* optimization strategies [7]. Multiphase composites with distributed nanostructures (created, for example, by high-energy milling) provide effective scattering centres for phonons [18]. The preparation of composites by mixing two sulphide phases to achieve high thermoelectric performance was described [19–26].

The aim of our paper is to verify the impact of tetrahedrite composite formation on thermoelectric performance. Two strategies have been applied, namely the addition of a foreign phase to tetrahedrite as well as the addition of product of its decomposition. For both strategies tools of mechanochemistry (*mechanical activation* (MA), *mechanochemical synthesis* (MS) and *mechanochemical leaching* (ML) were applied. The two mentioned strategies represent novelty of work where the new concept of composite formation can influence the thermoelectric performance of tetrahedrite. This concept broadens the knowledge about properties of tetrahedrite (without composites) described in our previous works [15,16].

2. Experimental

2.1. Materials

Natural mineral tetrahedrite $Cu_{12}Sb_4S_{13}$ from deposit Mária mine (Rožňava, Slovakia) (sample TELU-0) was used. Natural mineral contains a plethora of associated phases like SiO_2, $CuFeS_2$, FeAsS, and siderite $FeCO_3$(~20 %). When TELU-0 was modified by ML (see Methods), sample TELU-5 was obtained. The phase identification in the sample of natural tetrahedrite was determined by powder X-ray diffractometry using corresponding data from the JCPDS PDF database. The chemical composition was determined by classical analysis using coresponding dissolution media and an autoclave. Cu, Sb, S and Fe were determined in major amount. Moreover, Mn, As, Pb, Zn and Cd as minor elements were also determined.

Synthetic mineral tetrahedrite $Cu_{12}Sb_4S_{13}$ was obtained by MS from Cu, Sb and S precursors (99 % purity) in an industrial eccentric vibration mill (sample MS 1). The product after synthesis contains besides the main phase also associated famatinite Cu_3SbS_4 [15]. Its modifications by *mechanical activation* in a laboratory mill (sample MA 1) and its composite with 1% of mineral muscovite $KAl_2(AlSi_3O_{10})(OH)_2$ (sample MA 2) were also applied.

2.2. Methods applied for milled samples

2.2.1. Mechanochemical synthesis (MS)

MS was realized in an industrial excentric vibratory mill ESM 656–0.5 ks (Siebtechnik, Germany) working under the following conditions: 5 L milling chamber from hardened steel, milling balls from WC (diameter 35 mm, mass 30 kg), the amplitude of the milling vibrations 20 mm, a rotation speed of the mill 960 min^{-1}, argon atmosphere. The total feed of precursors into the mill was 100 g per batch, milling time was 720 min. The applied vibratory mill (Fig. 8) belongs to scalable vibratory mills which are capable to produce tens of kilograms of product. Its modification used in this work (so called „satellite mode“) enable us to copy the industrial milling regime and perform the milling in hundreds grams in an impact mode.

2.2.2. Mechanochemical activation (MA)

MA was performed in a laboratory planetary mill Pulverisette 6 (Fritsch, Germany) working under the following conditions: 250 mL milling chamber from tungsten carbide (WC), balls from WC (diameter 10 mm, mass 170 g), rotation speed 600 min^{-1}, the total feed into the mill 5 g per batch, milling time 60 min, argon atmosphere. The applied planetary mill (Fig. 8) works in a different regime in comparison with the mill described in part 2.2.1. Several milling modes are applied simultaneously like impact, shear, etc. However the scaling is problematic in this case.

2.2.3. Particle size distribution analysis and granulometric specific surface area

A Scirocco 2000 M (MALVERN Instruments, Great Britain) Mastersizer apparatus working in laser diffraction mode was employed to measure the particle size distribution in the range of 0.1–600 μm. Based on the measured data, the granulometric specific area was calculated [27]. All measurements were performed in triplicate.

2.2.4. Mechanochemical leaching (ML)

ML was performed in a stirred ball mill LME 075 (Netzsch, Germany) working under the following conditions: 500 mL milling chamber from hardened steel, balls from hardened steel (diameter 2 mm, mass 2000 g), rotation speed of the mill 1000 min^{-1}, the total feed into the mill 30 g per batch, milling time 60 min, 250 mL of leach solution (100 g/L Na_2S + 50 g/L NaOH) at temperature 60 °C was applied. The applied mill (Fig. 1) is capable to work in a wet mode (Na_2S/NaOH solution) in contrast to the mills described in 2.2.1 and 2.2.2 which are designed for a dry mode milling. The regime of a wet mode is needed to perform mechanochemical leaching.

2.2.5. X-ray diffractometry (XRD)

XRD patterns of MS and MA samples were collected for tetrahedrite samples using the D8 Advance diffractometer (Bruker, Germany) with the $Cu_{K\alpha}$ radiation in the Bragg–Brentano configuration. The generator was set up at 40 kV and 40 mA. The divergence and receiving slits were 0.3° and 0.1 mm, respectively. The XRD patterns were recorded with a

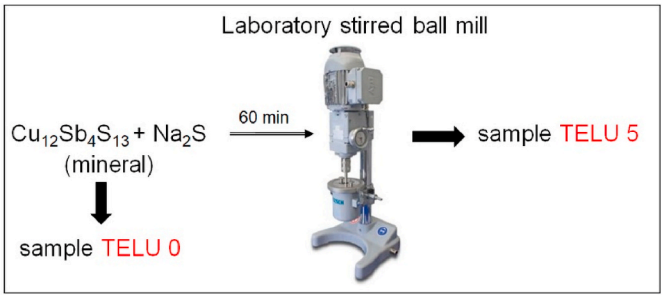


Fig. 1. Scheme of tetrahedrite *mechanochemical leaching*.

range of 2θ = 20–70° and step size 0.05°. The JCPDS PDF database for phase identification was utilized.

Empyrean PANalytical apparatus (Malvern, Panalytical, Worcestershire, UK) with CuK_α radiation was used for the characterization of ML samples. The equipment was working under the following conditions: range of 2θ = 20–90° step size 0.008°. For the assessment of data, X-Pert High Score software (Malvern, Panalytical Worcestershire, UK) was applied. The same equipments were used for sintered samples (see 2.3.).

2.2.6. Scanning electron microscopy (SEM)

The morphology and size of the powder particles after MA were investigated by using a scanning electron microscope Tescan Vega 3 LMU (Tescan, Czech Republic) using an accelerating voltage of 20 kV. To make the samples conductive, the powder was covered by a layer of gold on a fine coat ion sputter JFC 1100. To obtain information about the chemical composition of particles, the energy dispersive X-ray spectrometer (EDX) Tescan Bruker XFlash Detector 410 M (Bruker, Germany) was used.

The Thermoscientific Fischer Phenom XL scanning electron microscope equipped with an EDS analyzer was applied for samples after ML.

2.2.7. Thermal analysis

The thermal behaviour of samples after MS and MA were investigated by TG/DTG/DTA measurements using NETZSCH STA 449 F3 Jupiter (Netzsch, Selb, Germany). Measurements were performed over the temperature range 25–450 °C at a heating rate of 5 °C min^{-1} under an argon 5.0 (purity 99.999 %) atmosphere with a constant flow of 30 mL min^{-1}. As a crucible and reference sample Al_2O_3 was used.

2.3. Methods applied for sintered samples

2.3.1. Spark plasma sintering (SPS)

For SPS treatment of samples after ML self-designed apparatus was applied working under the following conditions: temperature 450 °C (heating rate 100 °C min^{-1}), time 20 min, pressure 50 MPa, vacuum 10^{-2} mbar. For sintering of samples graphite die was applied. The sintered pellets were 10 cm in diameter and 3 mm broad.

The powder after MS and MA was placed into a graphite die (inner diameter 10 mm) and sintered into pellets about 5 mm thick at 450 °C under 50 MPa (heating rate 100 °C min^{-1}), holding time 3 min in vacuum. The spark plasma sintering furnace model HP D10-SD (FCT Systeme GmbH, Germany) was applied.

2.3.2. Electrical conductivity and Seebeck coefficient

Measurements of the samples TELU 0 and TELU 5 were performed using self-made apparatus based on 4 - point DC method in the 293–673 K temperature range. These dynamic measurements were carried out under Ar atmosphere with temperature step 25 °C min^{-1}. The temperature was stabilized by 35 min annealing at each measurement point. For the Seebeck coefficient, the temperature gradient between the cold and hot site was set to 3 °C. The stability of the samples was investigated based on these measurements, conducted over four subsequent heating and slow-cooling cycles. Measurements of the samples MS 1, MA 1, and MA 2 were performed using the four-probe method on a ZEM - 3 measurement system (Ulvac-Riko, Japan).

2.3.3. Thermal conductivity

Thermal diffusivity and specific heat measurements were carried out with the use of an LFA 427 analyser (Netzsch, Germany) in an Ar atmosphere and an STA 449 F3 thermal analyzer (Netzsch, Germany), respectively. The pellets were cut into the required dimensions using a diamond-wire saw for electronic and thermal transport measurements. The measurements were performed from 323 K up to 673 K. Thermal diffusivity values (D) were obtained using a NETZSCH LFA HT 467 laser flash device. The thermal conductivity values of the samples were calculated with the relation $\kappa = DC_pd$, where C_p is the Dulong-Petit heat capacity and d is the experimental density of the sample.

3. Results and discussion

3.1. Properties of tetrahedrite modified by-products of mechanochemical leaching (ML)

The concept of this strategy is illustrated in Fig. 1. Tetrahedrite structure can be modified by alkaline leaching using the solution of Na_2S (see Methods). The process was performed to produce partly decomposed tetrahedrite forming a composite with its decomposition product (intrinsic mode). To evaluate the degree of decomposition, the amounts of antimony in solid product were determined by chemical analysis. While for a non-treated tetrahedrite was the content of Sb = 14.62 wt%, for mechanochemically leached tetrahedrite this value was reduced to Sb = 13.63 wt% as a consequence of partially leach out of antimony. The degree of tetrahedrite conversion is [(14.62–13.63)/14.62].100 % = 7%.

In technology, alkaline leaching is currently applied for tetrahedrite decomposition. Antimony is obtained in a soluble form and after its separation from non-soluble copper compounds, the antimony-free product is acceptable by copper producers [2]. As a result of this decomposition, copper is present in the form of chalcopyrite $CuFeS_2$ and/or chalcocite Cu_2S. Both copper sulphides are p- and/or n-type semiconductors attractive for thermoelectrics [28].

In Fig. 2., XRD patterns for sample TELU 0 are shown - powder after milling (a), the sintered pellet of the milled powder after SPS treatment (b) and the same pellet after thermoelectric treatment (c). The powder consists mainly of tetrahedrite $Cu_{12}Sb_4S_{13}$ (not assigned reflections), quartz SiO_2, siderite $FeCO_3$ and arsenopyrite FeAsS. The material is very stable and the composition after treatments has not changed. The presence of siderite as a second most abundant phase is evident. However, its composition is stable in all samples. Chalcopyrite and arsenopyrite as secondary phases are also evidenced.

Fig. 3 shows sample TELU 5 as a product of *mechanochemical leaching* of sample TELU 0. There is not much difference in phase distribution in comparison with Fig. 2. The main phase is again cubic tetrahedrite with a high amount of impurities (a). These impurities during the sintering process disappear (b,c) which may be related to ongoing reactions in this system. However, the ratio between the main reflexions of tetrahedrite and siderite is changing in favour of tetrahedrite, and after alkaline leaching, siderite is present in lower amount. It follows that, under applied experimental conditions, alkaline leaching is primarily focused on siderite dissolution. Evidence of new copper phases is not documented. In sample TELU 5 difficulties in the sintering of powder

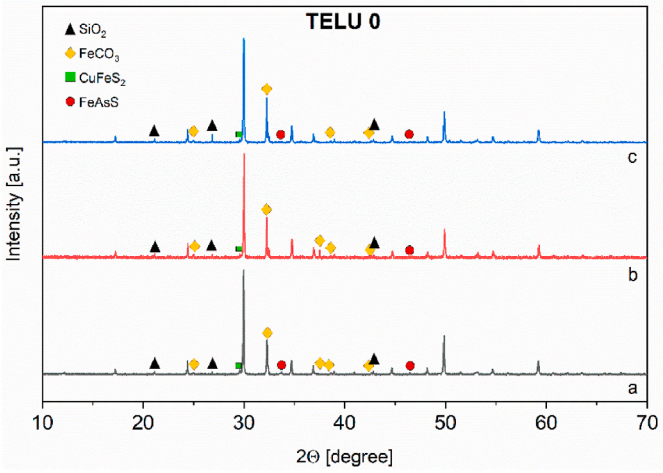


Fig. 2. XRD patterns of sample TELU 0: a - powder after milling, b - the pellet after SPS treatment, c - the same pellet after thermoelectric treatment.

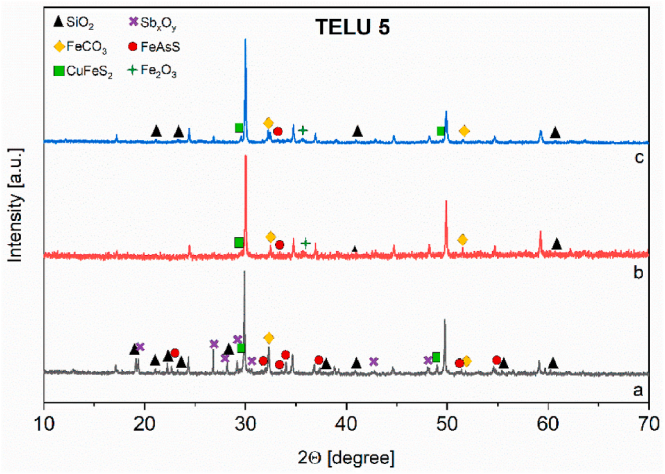


Fig. 3. XRD patterns of sample TELU 5: a - powder after milling, b - the sintered pellet of the milled powder after SPS treatment, c - the same pellet after thermoelectric treatment.

appeared. The material was very fragile and any mechanical treatment (cutting, polishing, etc.) was almost impossible to perform.

Thermoelectric measurements are illustrated in Figs. 4–7. The positive values of Seebeck coefficient *S* for samples TELU 0 and TELU 5 (Fig. 4) ranging between 120 and 180 μV/K are in agreement with the values typically reported for tetrahedrites with p-type conductivity. They tend to be slightly higher which indicates a slight stoichiometry deviation. All measurements were repeated 4 times. According to structural analysis, the sample TELU 0 was almost perfectly stable under working conditions. Only the first measurement seems to diverge from the rest (Fig. 4a), which is probably related to stress reduction after the sintering process. The results for sample TELU 5 (Fig. 4b) differ significantly in the subsequent cycles which also stays in good agreement with the literature. Notably, the subsequent measurements show a decreasing character of the Seebeck coefficient. We can speculate the reason is the creation of siderite decomposition products, mainly iron oxides. These species are hardly proven, especially when siderite and/or tetrahedrite decomposition products are still present after treatment (see Fig. 3a). Finally, the values of *S* are clearly lower compared to the non-treated TELU 0. Here, the semiconducting character of the TELU 5 is also less visible, as recorded values of the Seebeck coefficient are almost stable as a function of temperature.

In Fig. 5, the temperature dependences of the electric conductivity σ are shown. Again, for all repeated measurements, the plots for the TELU 0 sample are more homogeneous compared to TELU 5. The negative influence of oxide impurities can be clearly observed. Although these impurities have only partial influence on the Seebeck coefficient (Fig. 4) due to introducing minor changes in charge carrier concentration, they strongly affect the conductivity/mobility mechanisms in terms of both conduction across grain boundaries and through grains. According to the literature, typical electrical conductivities for tetrahedrites are 1–2.10^5 S m^{-1} [29]. Here, the values of σ for TELU 0 are 50 S m-1 in RT and 240 S m^{-1} in temperature 650 K, which are about 3–4 orders of magnitude lower. Electrical conductivities for the TELU 5 sample are even lower. The sample starts to be stable after 3–4 measurements and reaches final values at about 60–80 S m^{-1}. However, it is unusual for tetrahedrites that there is a strong increase of σ with increasing temperature, suggesting an additional conducting mechanism, linked to the existence of impurities.

It should be expected that a negative influence on electrical properties induces an opposite effect on heat transport. Indeed, the thermal conductivities for both samples (Fig. 6) are slightly lower compared to typical tetrahedrites (1.0–1.6 W m^{-1}K^{-1}). Again, it should be linked with the presence of the oxide compounds. The general picture of the thermoelectric material is defined by the values of figure of merit *ZT*. Unfortunately, the contribution of acceptable lower values of thermal conductivity is depressed with extremely low electrical conductivities, which determine the final values of *ZT* (Figs. 5 and 7).

3.2. *Properties of tetrahedrite prepared by mechanochemical synthesis and mechanochemical activation after addition of foreign phase (extrinsic mode)*

The concept of this strategy is illustrated in Fig. 8. Three types of samples were produced: sample MS 1 prepared by mechanochemical synthesis from Cu, Sb, and S precursors in an industrial mill (one-step milling), sample MA 1 prepared by laboratory milling of sample MS 1 (two-step milling) and sample MA 2 prepared in the same manner as sample MA 1 but with the addition of foreign phase muscovite (two-step milling). All three milled samples were subjected to consistent characterizations.

Particle size analysis (Fig. 9A) shows a great difference between MS 1 and/or MA 1 and MA 2 samples. In the first case, particles of a micrometre size are present and more abundant. The corresponding specific surface area value calculated from granulometric data for MS 1 was 0.23 m^2 g^{-1}. Samples MA 1 and MA 2 show different behaviour - there is a more pronounced size shift to nanometer dimensions with corresponding enhanced specific area values 0.525 m^2 g^{-1} and 0.527 m^{2}g^{-1} for MA 1 and MA 2, respectively.

Particle size analysis is supported by SEM results (Fig. 9B). While for MS 1 big agglomerates (characterized by the reduction in surface area) are observable, this is not the case for MA 1 and MA 2 where agglomerates are absent. From SEM observation of samples MA 1 and MA 2 the presence of smaller particles is evident.

The phase composition of samples under study is documented by XRD analysis (Fig. 9C) where XRD patterns recorded in a small 2 theta

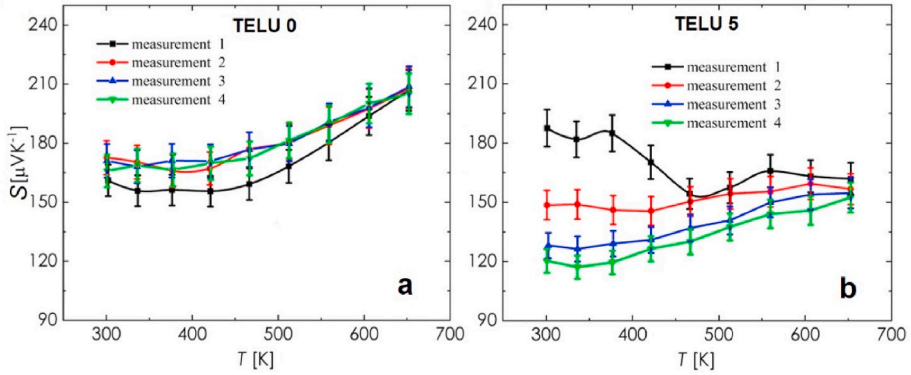


Fig. 4. Seebeck coefficient (*S*) as a function of temperature for sample TELU 0 (a) and sample TELU 5 (b).

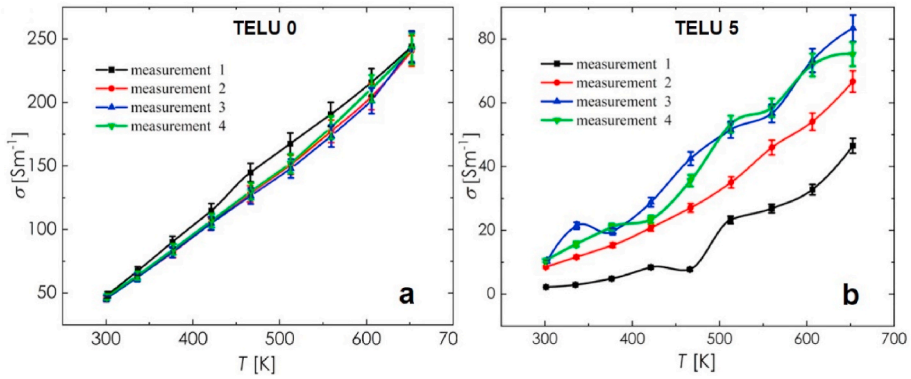


Fig. 5. Electrical conductivity (σ) as a function of temperature for samples TELU 0 (a) and TELU 5 (b).

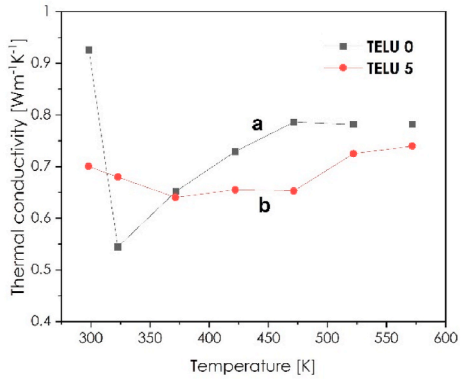


Fig. 6. Thermal conductivity (κ) as a function of temperature for samples TELU 0 (a) and TELU 5 (b).

range (26–34°) are shown. For MS 1 the main peaks of famatinite Cu_3SbS_4 and tetrahedrite $Cu_{12}Sb_4S_{13}$ are documented with approximately same heights. However, for samples, MA 1 and MA 2, the ratio of these peaks is changing in favour of famatinite.

The thermal stability of milled samples is illustrated by thermal analysis (TG, DTG, DTA) performed up to 450 °C (Fig. 9D). All curves for milled samples are very similar to each other. However, for samples, MA 1 and MA 2 (two-step milling), the onset of DTA peaks is shifted to lower temperatures in comparison with sample MS 1 (one-step milling). More information is available in Supporting Information (Figs. SI–1). Lowering the decomposition temperature as a consequence of increased energy of milling was observed for sulphides frequently [1].

The addition of muscovite (1%), which can be classified as an exotic secondary phase [30] (forming thus extrinsic mode of composite preparation) did not overcome the positive effect of milling.

XRD analysis of the three samples (after densification) in Fig. 10 indicates that the ratio of tetrahedrite/famatinite is quite similar, i.e. around 50/50. However, due to the presence of impurities, it was unfortunately not possible to perform accurate Rietveld refinement of the XRD data to extract more information on the structure.

Fig. 11 –12 show the electrical properties of the MS 1, MA 1 and MA 2 samples over the temperature range of 300–673 K. The Seebeck coefficient S (Fig. 11b) increases with temperature in agreement with the typical degenerate semiconducting behaviour of tetrahedrite or hole-doped Cu_3SbS_4 [31]. The electrical resistivity (ρ) (Fig. 11a) of MA 1 exhibits a consistent decrease as the temperature increases, whereas the electrical resistivity of MS 1 and MA 2 decrease with temperature till 200 °C and subsequently increase with temperature. The magnitudes of

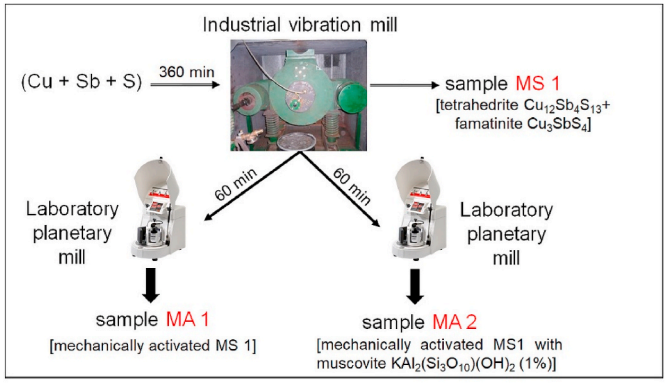


Fig. 8. Scheme of tetrahedrite mechanochemical synthesis and mechanochemical activation.

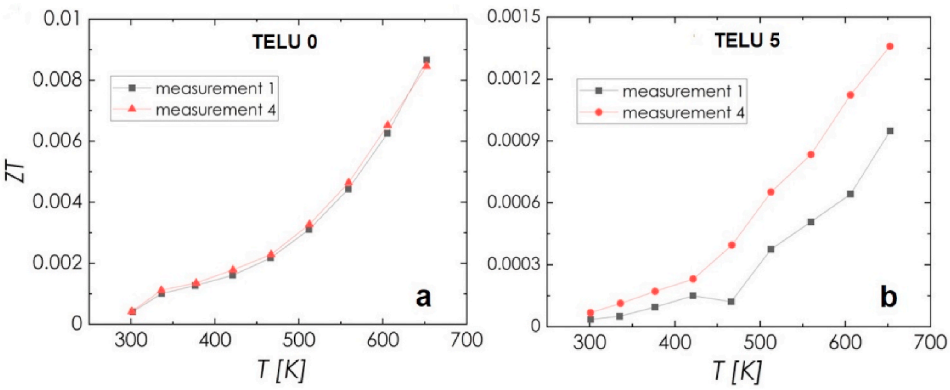


Fig. 7. Figure of merit *ZT* as a function of temperature for samples TELU 0 (a) and TELU 5 (b).

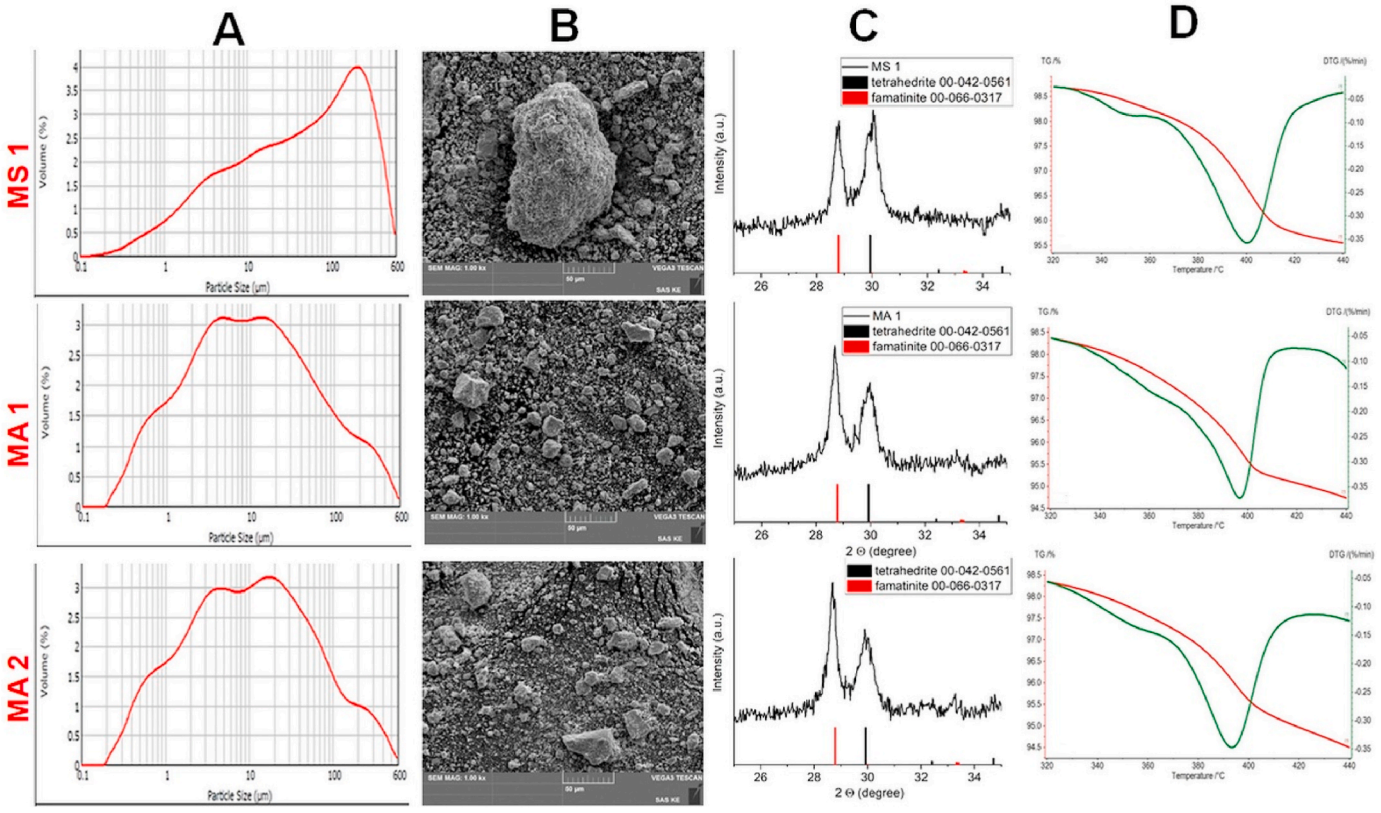


Fig. 9. Particle size distribution (A), scanning electron micrographs (B), X-ray diffraction patterns (C) and thermal analysis (D, red line- TG, green line- DTG)) of samples MS 1, MA 1 and MA 2.

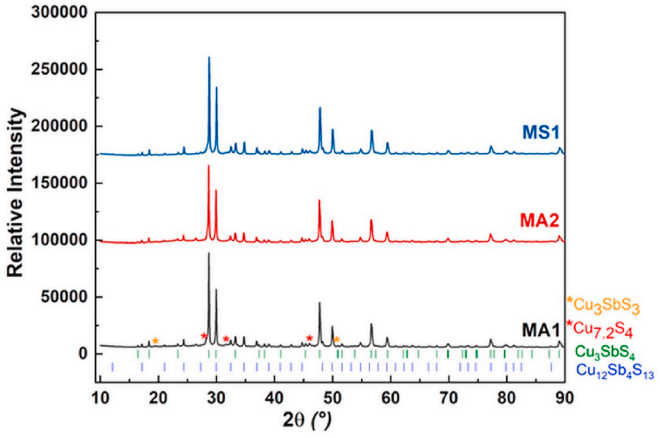


Fig. 10. XRD patterns of MS 1, MA 1 and MA 2 samples.

the Seebeck coefficient and electrical resistivity are both higher in MA 1 samples, indicating a lower carrier concentration in this sample, due to different stoichiometry. This leads to higher power factor values at high temperature for this sample.

The thermal conductivity data presented in Fig. 11c shows quite different behaviour for the three samples. It can be especially noticed a much lower thermal conductivity in sample MA 1. As for mechanochemical treatment, only samples MA 1 and MA 2 are comparable. While impact of mechanical energy is identical, the composition is different. In sample MA 1 only secondary milling was applied. In sample MA 2 the same procedure was applied. However, in this case before application of secondary milling the muscovite in small amount (1 %) was added. This behaviour seems related to the different electrical properties of this sample compared to the two others.

Due to the relatively high power factor and low thermal conductivity, MA 1 sample exhibits the highest *ZT* values with a maximum of 0.75 at 673 K (see Fig. 12)

Samples after thermal analysis were analysed by XRD (Figs. SI–2). Qualitatively, the same tetrahedrite $Cu_{12}Sb_4S_{13}$ and famatinite Cu_3SbS_4 phases were detected in samples before thermal analysis. No new phases were detected. However, two new phenomena were registered. Firstly, next to tetrahedrite $Cu_{12}Sb_4S_{13}$ (PDF 00-066-0328) present in sample MS 1, also tetrahedrite $Cu_{13.72}Sb_{4.09}S_{13}$ (PDF 00-024-1317) was identified for more energetically treated samples MA 1 and MA 2 (two-step milling). The tetrahedrite $Cu_{13.72}Sb_{4.09}S_{13}$ has less amount of sulphur as manifested by increased amounts of Cu and Sb. Secondly, the combined effect of more energetic mechanical treatment at two-step milling and the presence of evolved sulphur effect the mutual transformation of tetrahedrite to famatinite. While for sample MS 1 the ratio of main tetrahedrite and famatinite peaks is approximately equal, this is not the case for samples MA 1 and MA 2 where this ratio is shifted in favour of tetrahedrite (see Figs. SI–2).

4. Conclusions

Modification of tetrahedrite to form its composites is the main core of this paper. Tools of mechanochemistry have been applied, namely *mechanochemical leaching* (I) and *mechanical activation* (II).

In the first case (I), the composite of natural mineral tetrahedrite $Cu_{12}Sb_4S_{13}$ (p-type) with chalcopyrite $CuFeS_2$ (n-type) was formed. Chalcopyrite is present in the original sample (Fig. 2) as well as in product of mechanochemical leaching (Fig. 3) where its amount is slightly increased. However, the high amount of second parasitic phase siderite is several times higher (Figs. 2 and 3) and consequently also the amount of siderite decomposition products produced during sintering. This explains the low value of ZT. The combination of p- and n-type

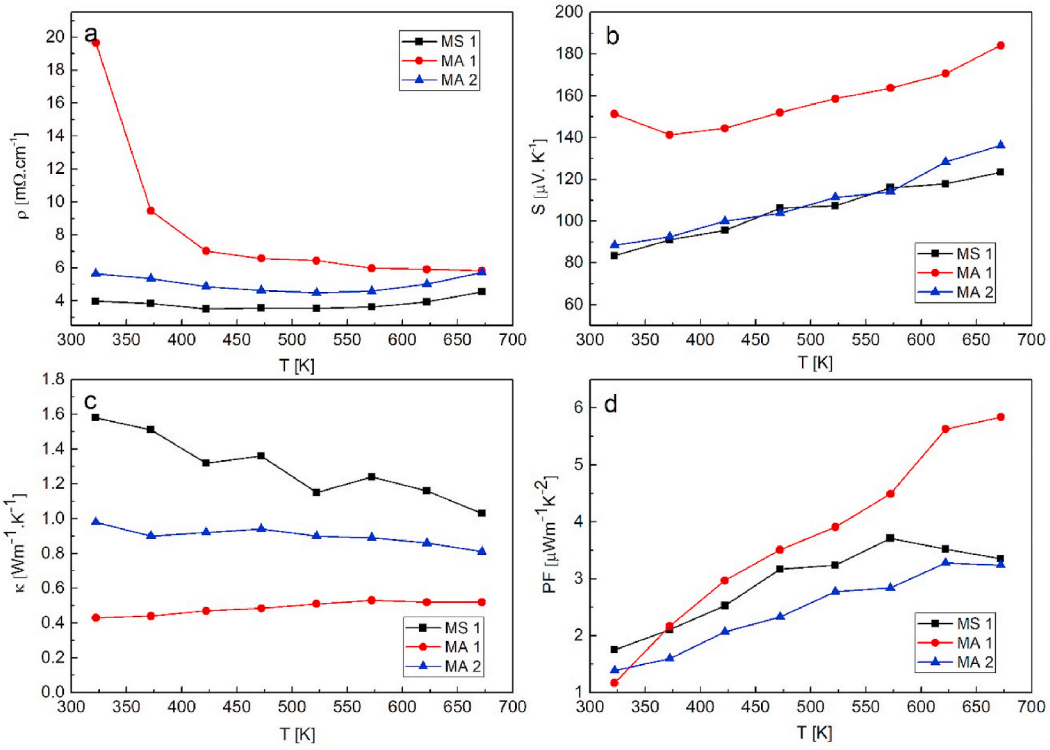


Fig. 11. Electrical resistivity ρ (a), Seebeck coefficient S (b), thermal conductivity κ (c) and power factor PF (d) as a function of temperature for samples MS 1, MA 1, and MA 2.

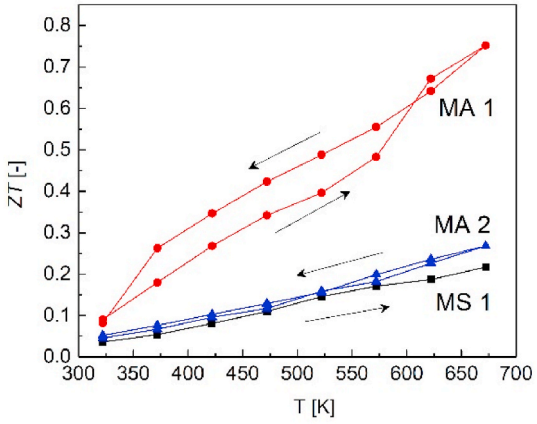


Fig. 12. Figure of merit *ZT* as a function of temperature for samples MS 1, MA 1, and MA 2.

semiconductors gives the value of $ZT = 0.0022$ @673 K. The composite manifests the low value of *ZT* for which extremely low electrical conductivity as a consequence of changes in tetrahedrite composition evoked by mechanochemical leaching is responsible.

In the second case (II), tetrahedrite $Cu_{12}Sb_4S_{13}$ synthesized by industrial milling was mixed with natural mineral muscovite $KAl_2(AlSi_3O_{10})(OH)_2$ and subsequently mechanically activated by laboratory milling. While the addition of muscovite did not give an extraordinary thermoelectric performance, the two-step milling (without the addition of muscovite) gives the value $ZT = 0.752$@673 K which belongs among the highest in the tetrahedrite community. This phenomenon is a consequence of a relatively high power factor and low thermal conductivity. The effect is promising because in this case the tetrahedrite/famatinite composite was applied in which famatinite is not effective thermoelectric substance [20].

CRediT authorship contribution statement

Peter Baláž: Writing – original draft, Supervision, Funding acquisition, Data curation, Conceptualization. **Arda Baran Burcak:** Investigation, Data curation. **Umut Aydemir:** Data curation. **Andrzej Mikula:** Writing – original draft, Investigation, Data curation. **Pawel Nieroda:** Investigation. **Matej Baláž:** Investigation. **Lenka Findoráková:** Investigation. **Radovan Bureš:** Investigation. **Viktor Puchý:** Investigation. **Murat Erdemoglu:** Funding acquisition. **Marcela Achimovičová:** Writing – original draft, Project administration, Funding acquisition. **Emmanuel Guilmeau:** Writing – review & editing, Writing – original draft, Methodology, Investigation, Data curation. **Sandy Al Bacha:** Data curation.

Declaration of competing interest

The authors declare that they have no known competing financial interests or personal relationships that could have appeared to influence the work reported in this paper.

Data availability

Data will be made available on request.

Acknowledgements

This work was supported by Slovak Agency VEGA (projects 02/0112/22, 02/0036/23). The support by the European Agency ERA-MIN 3 (project Potassial 27) is also acknowledged.

Appendix A. Supplementary data

Supplementary data to this article can be found online at https://doi.org/10.1016/j.solidstatesciences.2024.107497.

References

[1] P. Baláž, Extractive Metallurgy of Activated Minerals, 1, ed., Elsevier, Amsterdam, 2000, p. 292.

[2] P. Baláž, Mechanochemistry in Nanoscience and Minerals Engineering, Springer, Berlin, 2008, p. 413, https://doi.org/10.1007/978-3-540-74855-7.

[3] K. Suekuni, K. Tsuruta, T. Ariga, M. Koyano, Thermoelectric properties of mineral tetrahedrites $Cu_{10}Tr_2Sb_4S_{13}$ with low thermal conductivity, Appl. Phys. Express 5 (2012) 051201, https://doi.org/10.1143/APEX.5.051201.

[4] J. He, T. Tritt, Advances in thermoelectric materials research: looking back and moving forward, Science 357 (2017) 1369, https://doi.org/10.1126/science.aak9997.

[5] K. Suekuni, C.H. Lee, H.I. Tanaka, E. Nishibori, A. Nakamura, H. Kasai, H. Mori, H. Usui, M. Ochi, T. Hasegawa, M. Nakamura, S. Ohira-Kawamura, T. Kikuchi, K. Kaneko, H. Nishiate, K. Hashikuni, Y. Kosaka, K. Kuroki, T. Takabatake, Retreat from stress: rattling in a planar coordination, Adv. Mater. 30 (2018) 6 1706230, https://doi.org/10.1002/adma.201706230.

[6] A.F. Ioffe, Semiconductor Thermoelements and Thermoelectric Cooling, Infosearch Ltd., London, 1957, p. 182.

[7] Z. Li, C. Xiao, H. Zhu, Y. Xie, Defect chemistry for thermoelectric materials, Journal of the Am. Chem. Soc. 138 (2016) 14810–14819, https://doi.org/10.1021/jacs.6b08748.

[8] E. Isotta, B. Mukherjee, C. Fanciulli, N. Pugno, P. Scardi, Order-disorder transition in kesterite Cu_2ZnSnS_4: thermopower enhancement via electronic band structure modification, J. Phys. Chem. C 124 (2020) 7091–7096, https://doi.org/10.1021/acs.jpcc.0c00886.

[9] P. Baláž, M. Achimovičová, M. Baláž, P. Billik, Z. Cherkezova-Zheleva, J. Criado, F. Delogu, E. Dutková, E. Gaffet, F. Gotor, R. Kumar, I. Mitov, T. Rojac, M. Senna, A. Streletskii, K. Wieczorek-Ciurowa, Hallmarks of mechanochemistry: from nanoparticles to technology, Chem. Soc. Rev. 42 (2013) 7571–7637, https://doi.org/10.1039/C3CS35468G.

[10] J. Do, T. Friscic, Mechanochemistry: a force of synthesis, ACS Central Sci 3 (2017) 13–19, https://doi.org/10.1021/acscentsci.6b00277.

[11] F. Delogu, L. Takacs, Information on the mechanism of mechanochemical reaction from detailed studies of the reaction kinetics, J. Mater. Sci. 53 (2018) 13331–13342, https://doi.org/10.1007/s10853-018-2090-1.

[12] M. Kristl, S. Gyergyek, J. Kristl, Nanostructured nickel sulfides with different stoichiometries prepared by mechanochemical synthesis, Chalcogenide Lett. 15 (2018) 55–61.

[13] M. Baláž, Environmental Mechanochemistry, Springer, Switzerland, 2021. http://pi.lib.uchicago.edu/1001/cat/bib/12665666.

[14] Y. Lan, A. Minnich, G. Chen, Z. Ren, Enhancement of thermoelectric figure-of-merit by a bulk nanostructuring approach, Adv. Funct. Mater. 20 (2010) 357–376, https://doi.org/10.1002/adfm.200901512.

[15] P. Baláž, E. Guilmeau, N. Daneu, O. Dobrozhan, M. Baláž, M. Hegedüs, T. Barbier, M. Achimovičová, M. Kaňuchová, J. Briančin, Tetrahedrites synthesized via scalable mechanochemical process and spark plasma sintering, J. Eur. Ceram. Soc. 40 (2020) 1922–1930, https://doi.org/10.1016/j.jeurceramsoc.2020.01.023.

[16] P. Baláž, M. Achimovičová, M. Baláž, K. Chen, O. Dobrozhan, E. Guilmeau, J. Hejtmanek, K. Knížek, L. Kubíčková, P. Levinský, V. Puchý, M. Reece, P. Varga, R. Zhang, Thermoelectric Cu-S-based materials synthesized via a scalable mechanochemical process, ACS Sust. Chem. Eng. 9 (2021) 2003–2016, https://doi.org/10.1021/acssuschemeng.0c05555.

[17] A. Powell, Recent developments in Earth-abundant copper-sulfide thermoelectric materials, J. Appl. Phys. 126 (2019) 100901, https://doi.org/10.1063/1.5119345.

[18] N. Jia, X. Tan, J. Xu, Q. Yan, M. Kanatzidis, Achieving enhanced thermoelectric performance in multiphase materials, Accounts Mater. Res. 3 (2022) 237–246, https://doi.org/10.1021/accountsmr.1c00228.

[19] X. Lu, D. Morelli, Y. Xia, F. Zhou, V. Ozolins, H. Chi, X. Zhou, C. Uher, High performance thermoelectricity in Earth-abundant compounds based on natural mineral tetrahedrites, Adv. Energy Mater. 3 (2013) 342–348, https://doi.org/10.1002/aenm.201200650.

[20] X. Lu, D. Morelli, Natural mineral tetrahedrite as a direct source of thermoelectric materials, Phys. Chem. Chem. Phys. 15 (2013) 5762–5766, https://doi.org/10.1039/C3CP50920F.

[21] P. Levinský, C. Candolfi, A. Dauscher, J. Tobola, J. Hejtmánek, B. Lenoir, Thermoelectric properties of the tetrahedrite-tennantite solid solutions $Cu_{12}Sb_{4-x}As_xS_{13}$ and $Cu_{10}Co_2Sb_{4-y}As_yS13$ ($0 \leq x$, $y \leq 4$), Phys. Chem. Chem. Phys. 21 (2019) 4547–4555, https://doi.org/10.1039/C9CP00213H.

[22] P. Baláž, E. Dutková, P. Levinský, N. Daneu, L. Kubíčková, K. Knížek, M. Baláž, J. Navrátil, J. Kašparová, V. Ksenofontov, A. Moller, J. Hejtmánek, Enhanced thermoelectric performance of chalcopyrite nanocomposite viac co-milling of synthetic and natural minerals, Mater. Lett. 275 (2020) 128107, https://doi.org/10.1016/j.matlet.2020.128107.

[23] Y. Zhao, Y. Gu, P. Zong, L. Pan, L. Zhang, K. Koumoto, Y. Wang, High thermoelectric performance of Co-doped Cu_2SnS_3-attapulgite nano-composites achieved by synergetic manipulation of electrical and thermal transport properties, J. Alloy Compd. 887 (2021) 161338, https://doi.org/10.1016/j.jallcom.2021.161338.

[24] A. Mikula, K. Mars, P. Nieroda, P. Rutkowski, Copper chalcogenide-copper tetrahedrite composites-a new concept for stable thermoelectric materials based on the chalcogenide system, Mater 14 (2021) 2635, https://doi.org/10.3390/ma14102635.

[25] M. Li, Y. Liu, Y. Zhang, X. Han, K. Xiao, M. Nabahat, J. Arbiol, J. Llorca, M. Ibanez, A. Cabot, PbS-Pb-Cu_xS composites for thermoelectric application, ACS Appl. Mater. Inter. 13 (2021) 51373–51382, https://doi.org/10.1021/acsami.1c15609.

[26] P. Levinský, P. Ventrapati, A. Dauscher, J. Hejtmánek, C. Candolfi, P. Lenoir, Achieving high thermoelectric performance in mixed natural-synthetic tetrahedrites, Chemnanomat 8 (2022) e202200364, https://doi.org/10.1002/cnma.202200364.

[27] T. Allen, Particle Size Measurement, 3th ed., Springer, New York, 1981.

[28] P. Lemoine, G. Guelou, B. Raveau, E. Guilmeau, Crystal structure classification of copper-based sulfides as a tool for the design of inorganic functional materials, Angew. Chem. Int. Edit. 61 (2022) e202108686, https://doi.org/10.1002/anie.202108686.

[29] R. Chetty, A. Bali, R. Mallik, Tetrahedrites as thermoelectric materials: an overview, J. Mater. Chem. C 3 (2015) 12364–12378, https://doi.org/10.1039/C5TC02537K.

[30] Y. Zheng, T.J. Slade, L. Hu, X.Y. Tan, Y. Luo, Z.-Z. Luo, J. Xu, Q. Yan, M. G. Kanatzidis, Defect engineering in thermoelectric materials: what have we learned? Chem. Soc. Rev. 50 (2021) 9022–9054, https://doi.org/10.1039/D1CS00347J.

[31] K. Suekuni, K. Tsuruta, M. Kunii, H. Nishiate, E. Nishibori, S. Maki, M. Ohta, A. Yamamoto, M. Koyano, High-performance thermoelectric mineral $Cu_{12-x}Ni_xSb_4S_{13}$ tetrahedrite, J. Appl. Phys. 113 (2013) 043712, https://doi.org/10.1063/1.4789389.